Direct Evidence of Molecular Aggregation and Degradation Mechanism of Organic Light-Emitting Diodes under Joule Heating: an STM and Photoluminescence Study

Jian-Ru Gong,[†] Li-Jun Wan,* Sheng-Bin Lei, and Chun-Li Bai*

Institute of Chemistry, Chinese Academy of Sciences, Beijing 100080, China

Xiao-Hong Zhang

Nano-organic Photoelectronic Laboratory, Technical Institute of Physics and Chemistry, Chinese Academy of Sciences, Beijing 100080, China

Shuit-Tong Lee*

COSDAF and Department of Physics and Materials Science, City University of Hong Kong, Hong Kong SAR, China

Received: August 4, 2004; In Final Form: November 5, 2004

The Joule heating effect on electroluminescent efficiency is important in the degradation origin of organic light-emitting diodes (OLED). Scanning tunneling microscopy (STM) and photoluminescence (PL) measurements were performed on the guest molecule **BT** (1,4-bis(benzothiazole-vinyl) benzene), host molecule **TPBI** (2, 2′,2″-(1,3,5-phenylene)tris-[1-phenyl-1H-benzimidazole]), and their mixture deposited on an HOPG surface to study the OLED degradation mechanism due to thermal heating. At room temperature, **BT** and **TPBI** in the mixed layer show good compatibility and high PL intensity, but at higher temperatures, they show phase separation and aggregation into their own domains and a concomitant decrease in PL intensity. The PL intensity loss suggests ineffective energy transfer from **TPBI** to **BT** due to phase separation, which may cause OLED degradation. Scanning tunneling spectroscopy (STS) results show that the band gaps of **TPBI** and **BT** remain unchanged with the annealing temperature, suggesting that the heat-induced decay of OLED is related to the interfacial structural change rather than the respective molecular band gap. The results provide direct evidence showing how the molecular structures of the mixed layer vary and affect the PL intensity due to temperature.

Introduction

Organic light-emitting diodes (OLED) have attracted great interest because of their potential application in low-cost, full-color, large-area, and flat-panel displays.[1] Interfacial phenomena are crucial to the performance and stability of OLED, which represent a challenging and important area of OLED science and technology and have been a subject of intensive theoretical and experimental study.[2−4] For example, the interfacial structures influence charge injection and yield varying degrees of improved device performance in terms of turn-on voltage, maximum luminance, and quantum efficiency. To date, a variety of interfacial treatment and preparation methods has been applied to the cathode/organic and anode/organic junctions. Some recent advances have been achieved using the self-assembling technique,[5,6] which could produce an exactly controlled film. On the other hand, the charge injection, transportation, and luminescent mechanisms in OLED are well-elucidated with interfacial structures. Marks et al. reported that chlorosilane-functionalized triarylamines and biphenyls assemble themselves into well-ordered and smooth layers via strong covalent bonds. The OLED so-prepared emits blue light as bright as the glow of a standard television set.[7,8] Zuppiroli et al. studied the morphology of organic electroactive film vapor deposited on indium tin oxide (ITO) electrodes at different temperatures and demonstrated that self-assembled monolayers of appropriate molecules are very efficient in improving the interface morphology.[9] Brinkmann et al. discussed the correlation between the molecular packing and the fluorescence spectral features of tris(8-hydroxyquinoline) aluminum (Alq_3) in different polymorphic crystalline phases.[10] The morphology, surface, and interfacial electronic structure have been investigated intensively using techniques such as scanning electron microscopy (SEM),[9] Fourier transform infrared reflection−absorption spectroscopy,[11] ultraviolet photoelectron spectroscopy (UPS),[12] inverse photoemission spectroscopy (IPES), and X-ray photoelectron spectroscopy (XPS).[13]

Despite much improved device performance, an insufficient lifetime remains one of the primary issues limiting the widespread commercial use of OLED. Consequently, an understanding of the phenomena related to the degradation mechanisms of OLED such as the compatibility and thermostability of the host−guest materials in an amorphous state is still of broad interest.[1] Among the various factors that may contribute to the degradation phenomena in OLED, the Joule heating effect on electroluminescent efficiency and lifetime is considered an important factor.[14] Lifetime reduction of 1 or 2 orders of magnitude has generally been found for OLED operated at 60−70 °C as compared with those operated at room temperature.[1] Therefore, the investigation of a Joule heating effect on OLED degradation is of interest. Similarly, the detailed understanding of interfacial structural changes with temperature in a nanometer scale is also of interest.

* Corresponding authors. For L.-J. W. Tel./fax: +86-10-62558934; e-mail: wanlijun@iccas.ac.cn.

† Also in Graduate School of Chinese Academy of Sciences.

10.1021/jp046509o CCC: $30.25
Published on Web 01/13/2005

Scanning tunneling microscopy (STM) is a powerful surface characterization technique[15] and has been used to generate electroluminescence from Alq_3 on Au(111) substrates, which showed the emission spectra to be highly dependent on the local structural features of the thin film.[16] In the present study, we used STM to investigate the self-assembling behavior of the guest molecule **BT** (1,4-bis(benzothiazole-vinyl) benzene), host molecule **TPBI** (2, 2′,2″-(1,3,5-phenylene)tris-[1-phenyl-1H-benzimidazole]), and their mixture deposited on the HOPG surface. Thermal treatment was employed to simulate the Joule heating effect. The host−guest mixed layer of **TPBI** and **BT** was found to have good compatibility at room temperature. However, phase separation was observed at increasing temperature, with a concomitant decrease in emission intensity, as confirmed by the photoluminescence (PL) spectra. Furthermore, the scanning tunneling spectroscopy (STS) measurements show that the characteristic band gap of **TPBI** and **BT** remain unchanged with the annealing temperature. This result further supports that ineffective host-to-guest energy transfer is responsible for the decay of OLED due to phase separation.

Experimental Procedures

The guest material benzothiazole derivative **BT** and host material **TPBI** were synthesized using published methods.[17,18] For comparison, another benzothiazole derivative, ***m*-BT** (1,4-bis(*m*-methyl-benzothiazole-vinyl) benzene, was also used to acquire molecular images. The chemical structures of the three molecules are shown in Scheme 1. A drop (2 μL) of solution

SCHEME 1: Chemical Structures of the Compounds Studied

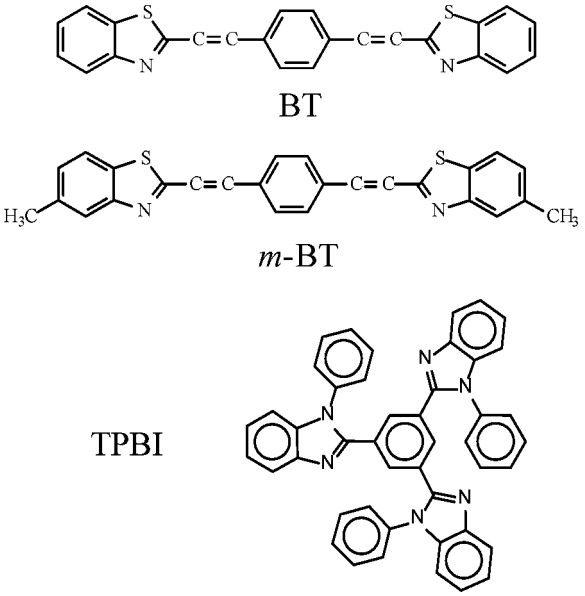

containing **BT**, ***m*-BT**, **TPBI** (the concentration for the three molecules is less than 1 mM), or a mixture of 2 wt% **BT** in **TPBI** (the concentration of **TPBI** is less than 1 mM) was placed on a freshly cleaved atomically flat surface of highly oriented pyrolytic graphite (HOPG) (quality ZYB). A self-organized film was formed after the evaporation of solvent. We do not use the spin-coating method. The thickness of the films on HOPG for STM observation should be the same. To keep the reproducibility of the sample, we used the solutions in the same concentration and the same area of HOPG. Toluene (HPLC grade, Aldrich) was used as a solvent for preparing all solutions.

A Nanoscope IIIa SPM (Digital Instruments, Santa Barbara, CA) was employed to carry out the STM experiments using a standard constant current mode under ambient conditions. STM tips were mechanically cut Pt/Ir wire (90:10). All the STM images are presented without further processing. The tunneling conditions used are given in the corresponding figure captions. To ensure the result was reproducible, the experiment was repeated many times, and several different areas of the adlayers were imaged.

Tunneling spectra were acquired in an STS mode provided by SPM 3.2 software (Digital Instruments) with the feedback loop disabled. A Model SR 810 DSP Lock-in Amplifier provided the bias modulation externally. Another computer recorded the change in the tunneling current and d*I*/d*V* as a function of bias voltage at a fixed tip−sample separation. In this way, the noise was apparently reduced. d*I*/ d*V* curves were measured quickly (in an order of 500 ms) to minimize thermal drift of the tip and sample during data acquisition. The points where the local d*I*/d*V* data have been obtained are indicated in the simultaneously obtained STM image. Therefore, the occurrence of drift in the *x*,*y*-plane can be identified. The presented spectra, which have constant tunneling conditions $I = 336$ pA and $V = 1.09$ V, are averaged but not filtered.

The optimum doping concentration typically varies from a fraction of 1% to a few percent. Low doping the **BT** concentration may lead to insufficient emission due to lack of emitters, while a high concentration may lead to exciton quenching. Therefore, the concentration of **BT** molecules available in the transfer process plays a crucial role. Here, a concentration of 2 wt % **BT** was chosen, according to the previous research.[17] Thermal annealing of the 2 wt% **BT** and **TPBI** mixed layer was carried out in air at different temperatures of 80−180 °C for 1 h. The surface morphology of the mixed layer was investigated by STM after the sample was naturally cooled to room temperature. For photoluminescence measurement, the fluorescence spectra were taken with a Fluorolog-3 spectrofluorometer. The excitation wavelength was 330 nm. The sample preparation was identical with that for STM observation, while a quartz substrate was used instead of HOPG.

A brief explanation of the whole experimental process is illustrated in Scheme 2.

Results and Discussion

1. Morphology of Self-Assembled BT, *m*-BT, and TPBI Adlayers. The individual molecular adlayers were first prepared on the HOPG surface. The structures and molecular features of the so-prepared adlayers were investigated with in-situ STM.

BT and *m*-BT Adlayers. Figure 1a shows a large-scale STM image acquired on a **BT** adlayer. It can be seen that **BT** molecules adsorbed on HOPG self-organize into a well-defined adlayer consisting of regular molecular rows with bright bands and dark stripes over a large area. The average size of the molecular domains is larger than 100 × 100 nm. The high-resolution STM image in Figure 1b reveals the structural details of the adlayer with submolecular resolution. The molecular arrangement in the **BT** adlayer can be observed. From the chemical structure and molecular size, it is confirmed that each molecule appears in a set of bright spots as illustrated by a superimposed model. The molecules adsorbed on the HOPG surface with the same orientation. The distance between two molecular rows is measured to be 2.6 ± 0.1 nm, and the spacing between two nearest molecules along the row is 0.7 ± 0.1 nm. Two molecular rows **A** and **B** cross each other with an angle of 114 ± 2°. A unit cell is outlined in Figure 1b. On the basis of the intermolecular distance and orientation, a molecular model is tentatively proposed in Figure 1c. The structural model is consistent with the results obtained from the STM observation.

SCHEME 2: Whole Experimental Process[a]

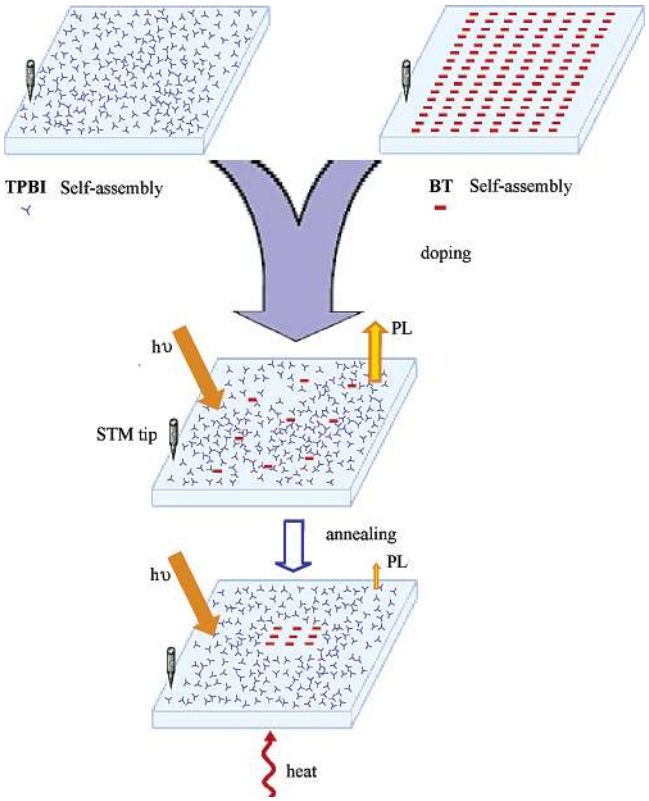

[a] After **BT** and **TPBI** adlayers were imaged, the 2 wt % **BT** and **TPBI** multiplayer was homogeneously prepared. The multilayer was annealed within the range of 80−180 °C for 1 h. The structural and photoluminescent changes with temperature were investigated by STM and spectrofluorometry, respectively.

The molecule ***m*-BT** is a derivative of **BT** with the attachment of two methyl groups. A well-ordered monolayer is observed for ***m*-BT** molecules. Figure 2a is a typical STM image showing the adlayer in a large area. Similar to **BT**, ***m*-BT** molecules self-organize into a regular array. The array is composed of parallel molecular rows. The high-resolution STM image in Figure 2b reveals the arrangement of ***m*-BT** molecules on the graphite surface with submolecular resolution. Each molecule appears in a rectangular shape. The molecular details such as the aromatic benzene ring can be resolved in the image. As compared to the chemical structure of the ***m*-BT** molecule, the bright parts in a molecule correspond to the aromatic rings of the ***m*-BT** molecule, while the methyl groups with low electronic density have a lower contrast than the aromatic ring in the image. A molecular model is superimposed on the image. The distance between two molecular rows measured from the STM image is 2.9 ± 0.1 nm, which is longer than that of **BT** due to the existence of methyl groups. The intermolecular distance of 0.7 ± 0.1 nm along row **A** is close to that of **BT**. Two molecular rows **A** and **B** cross each other at 106° with an experimental error of ±2°. A molecular model is tentatively proposed in Figure 2c, giving a visual representation of the monolayer structure. A unit cell with parameters $a = 0.7$ nm, $b = 2.9$ nm, and $\alpha = 106°$ is shown in Figure 2b,c. In this model, each molecule adsorbs onto the HOPG surface in a flat-lying orientation. The molecules self-organize into a well-defined two-dimensional adlayer. From the chemical structure, the **BT** or ***m*-BT** molecule has an aromatic π system. Through the interaction between the π electrons and the graphite surface, the molecules adsorb on the substrate and take a flat-lying orientation.

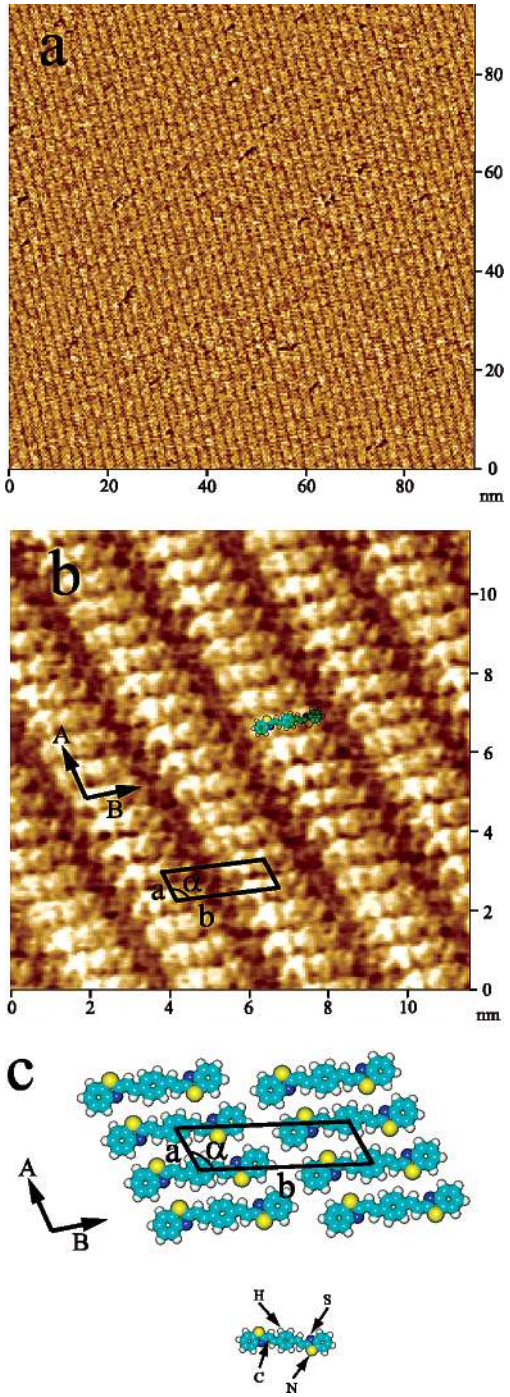

Figure 1. (a) STM topography of large-scale BT assembly recorded with $I = 1.01$ nA and $V = 727$ mV. (b) High-resolution STM image of BT molecules recorded with $I = 758$ pA and $V = 648$ mV. (c) Structural model for the 2-D packing of BT molecules.

TPBI Adlayer. The ordered arrangement of benzothiazole derivatives indicates that a relatively strong intermolecular interaction exists in the monolayer. This strong intermolecular interaction has also been verified by Zhang's emission and absorption spectra.[17] On the other hand, the planar molecules of **BT** and ***m*-BT** favor the adsorption onto the HOPG surface and result in high stability of the adlayers. However, because of the steric configuration of **TPBI**, the overlap of the π systems of **TPBI** and the graphite substrate is inhibited. Therefore, it is difficult for **TPBI** molecules to form a two-dimensional ordered adlayer. Although great effort was made, such as changing molecular concentration, solvents, and imaging parameters, no ordered **TPBI** adlayer could be prepared and imaged. Figure 3

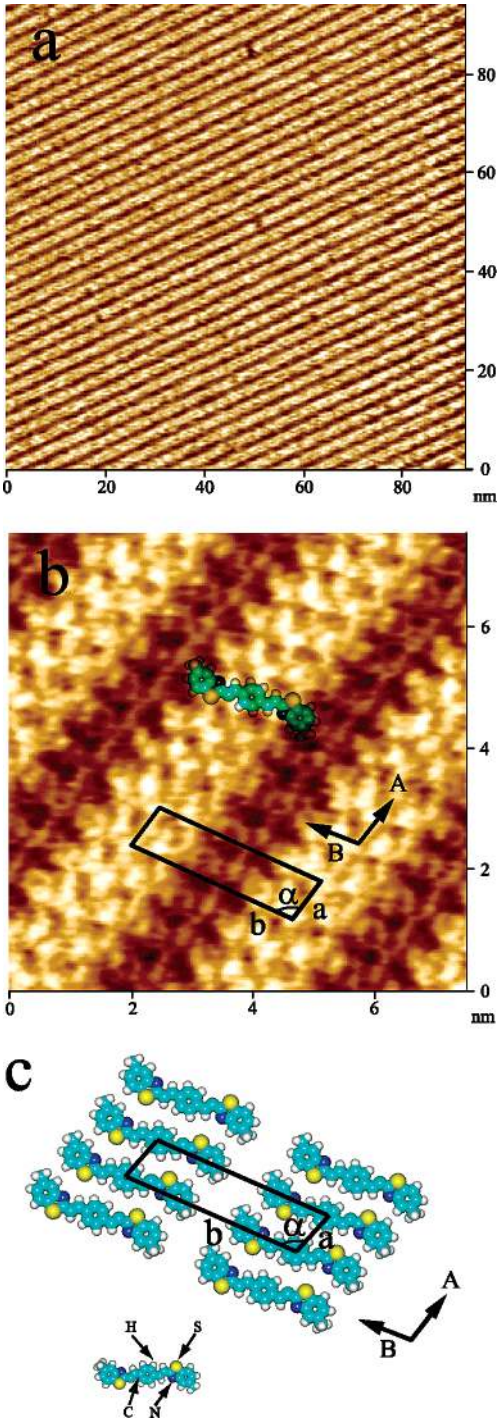

Figure 2. (a) STM topography of large-scale ***m*-BT** assembly recorded with $I = 1.01$ nA and V = 405 mV. (b) High-resolution STM image of ***m*-BT** molecules recorded with $I = 959$ pA and $V = 800$ mV. (c) Structural model for the 2-D packing of ***m*-BT** molecules.

is a typical STM image recorded on the **TPBI** adlayer, which appears as an amorphous layer.

Mixed Layer of TPBI and BT. Figure 4a shows a representative STM image of the mixed layer of 2 wt % **BT** in **TPBI** at room temperature. The image shows that **TPBI** and **BT** are homogeneously mixed together (the right corner enlargement gives a more clear image for comparison), revealing good compatibility between the molecules. However, no ordered feature can be seen in the image.

After the preparation and observation of various molecular adlayers, the relationship between the adlayer structure and the photoluminescent intensity was studied. High-temperature annealing was employed to the previously mixed layer, and the consequent structural change was observed from STM images.

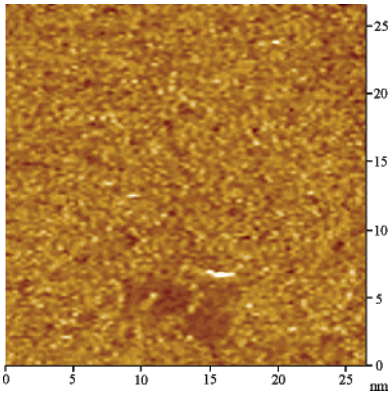

Figure 3. TPBI adlayer STM image on HOPG recorded with $I = 700$ pA and $V = 928$ mV.

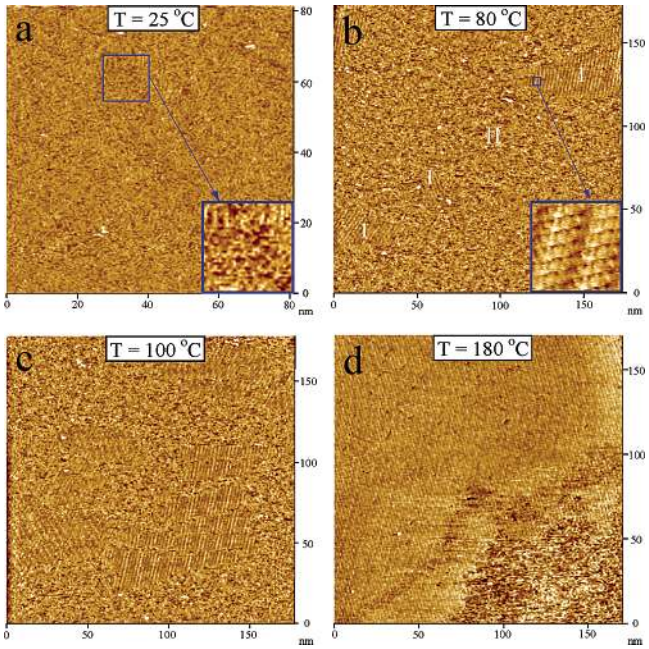

Figure 4. (a−d) Series of STM image of BT and TPBI mixed adlayer on HOPG with different annealing temperature, recorded with $I = 700-948$ pA and $V = 590-928$ mV. (b) Coexistence of phase I (domain of pure BT) and phase II (domain of TPBI or mixed TPBI and BT). The inset is the high-resolution image in phase I.

2. Structure and Photoluminescence of the Mixed Layer of TPBI and BT under Joule Heating. Doping dyes with a high fluorescent quantum yield into host materials with good carrier-transporting properties is a useful method to improve the electroluminescent efficiency of OLED. This also provides a simple way to tune the emitting color of OLED. To date, most of the high-efficiency OLEDs are made this way, which frequently also leads to enhanced device operational stability.[19,20]

In the present study, **BT** guest molecules were doped into **TPBI** host molecules to form a mixed layer to simulate the emissive layer in an OLED. Thermal treatment was employed to simulate the Joule heating effect on OLED, like cutting off the OLED power after a period of device operation. The morphology change of the mixed layer as a function of annealing temperature from 25 to 180 °C was investigated by STM. The PL spectra at room temperature (25 °C) showed the emission peak of **BT** film but no apparent emission peak (about 400 nm) of **TPBI** film, confirming that the emission is from the dopant. For a comparison, the PL spectra of **TPBI** and **BT** are shown

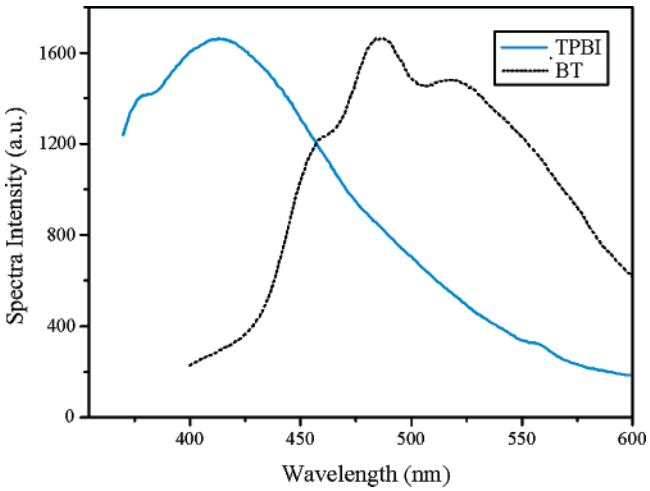

Figure 5. Photoluminescence spectra of BT and TPBI film at room temperature. Excitation wavelength is 330 nm.

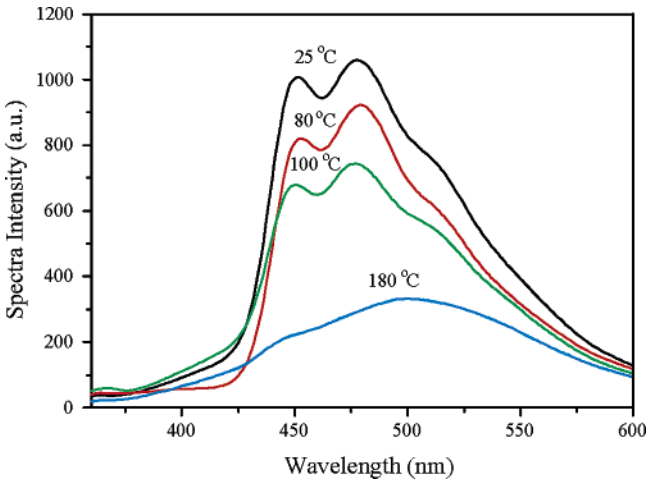

Figure 6. Photoluminescence spectra of 2 wt % BT and TPBI mixed film at different annealing temperature. Excitation wavelength is 330 nm.

in Figure 5, respectively.[17,21] The result suggests that energy transfer from **TPBI** to **BT** should be effective, and doping **BT** into **TPBI** may be expected to form an efficient emitting layer.

The PL spectra of the **BT**-doped **TPBI** layer at different annealing temperatures are shown in Figure 6. At room temperature, two intense peaks are clearly seen in the PL spectra. One peak is located at 450 nm and another at 478 nm. The results are consistent with the previous study.[17] At room temperature, the **TPBI** and **BT** molecules are homogeneously mixed, showing good compatibility as depicted in the STM image in Figure 4a. We made STM measurements on several places in a large size and obtained almost the same image as Figure 4a, demonstrating no phase separation in the mixed layer.

After annealing at 80 °C, a structural change in the mixed layer has been observed, as revealed by the typical STM image in Figure 4b. Although most of the imaged area remains in the disordered structure (phase II), several small domains (phase I) consisting of ordered molecular rows are seen, indicating the occurrence of phase separation. The inset in Figure 4b shows a high-resolution STM image that reveals the molecular feature and arrangement in the ordered domains. From the resemblance of this image to the individual molecular images in Figure 1, it can be concluded that phase I is the **BT** adlayer. In this case, the PL intensity decreased considerably as shown in Figure 6, although the two peaks at 450 and 478 nm are still evident. The effect of phase separation on photoluminescence can be clearly seen. Raising the annealing temperature to 100 °C, the PL intensity reduced further and reached about 2/3 of that at room temperature (25 °C). At this point, the STM image in Figure 4c shows that the domains of **BT** have grown larger. The enlargement of domains is due to merging and/or growth of smaller domains as a result of continued aggregation of **BT** molecules. In the scanned area, almost half of the adlayer shows the ordered structure of **BT** molecules. After annealing at 180 °C, the ordered **BT** phase with a domain size of more than 100 nm could clearly be discerned, as shown in Figure 4d, where the regular molecular rows are clearly seen. Note that the concentration of **BT** in the multiplayer is only 2 wt %. In the image of Figure 4d, the scanned area almost is fully covered by ordered **BT** molecules, although most of the remaining area of the layer is still covered by the **TPBI** molecules in a disordered structure. The results show that the annealing has induced extensive **BT** molecule aggregation, forming its own domains, and possibly resulting in complete phase separation. The structural evolution of the mixed layer with temperature is sequentially and visually revealed by STM images in Figure 4.

Furthermore, after annealing at 180 °C, the PL intensity greatly decreased, and the two featured peaks disappeared as shown in Figure 6, indicating a drastic reduction of host−guest energy transfer efficiency. The decrease of energy transfer from **TPBI** to **BT** suggests that phase separation annihilates radiative centers, which are responsible for the loss of EL efficiency. The decrease of PL intensity in the mixed layer is well-correlated to the STM results of the same layer with annealing temperature. According to Förster's energy transfer model, there is an available distance R (1−10 nm), or capture radius, of a guest molecule for efficient host−guest energy transfer.[22] The occurrance of phase separation increases the host−guest distance beyond R and makes the energy transfer ineffective. This explanation is widely accepted for illustrating the OLED failure mechanism. Our result provides direct evidence at the molecular level to understand the macroscopic decay phenomenon of OLED. Apparently, the host−guest energy transfer will be difficult in a film with separated phases where the host and guest molecules are positioned in different domains.

3. Electronic Property of Self-Assembled Adlayers. OLED usually contains an organic electroluminescence medium with one or more layers sandwiched by two electrodes. Charge is injected into the HOMO (highest occupied molecular orbital) at the anode and the LUMO (lowest unoccupied molecular orbital) at the cathode. These injected charges migrate in the applied field until they recombine and produce a radiative state. The OLED structure and energy level diagram are simplified in Scheme 3a. With the recent progress in high-efficiency OLEDs, many experimental and theoretical efforts have been undertaken to elucidate the underlying fundamental physical processes. The knowledge of the relative alignment of the energy levels at interfaces between organic materials is crucial to understanding the OLED operation and efficiency. The deep understanding of the electronic structure always requires the knowledge of geometrical structures and comprehensive characterization of the samples. Frequently, organic molecules adsorb weakly on a surface only via van der Waals interaction. The HOMO and LUMO are usually localized in each molecule with narrow intermolecular bandwidths of <0.1 eV. Thus, the electronic structure of an organic solid largely preserves that of a molecule.[23]

Here, we apply the STS technique to probe local property. In this technique, the STM tip functions as a movable electrode

SCHEME 3[a]

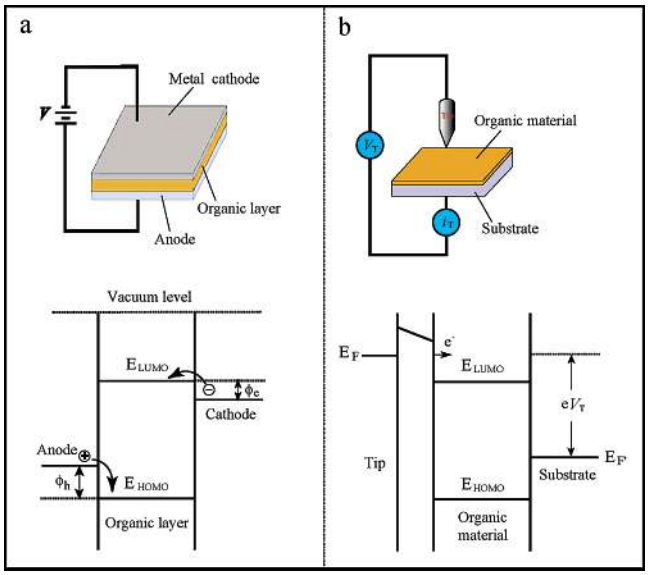

[a] (a) The structure and energy diagram for OLED. Assuming that the energy levels correspond to a common vacuum level, φ_h and φ_e are the hole and electron barriers. (b) A typical STM configuration and energy diagram, in which charge injection into the organic material occurs via tunneling through a vacuum barrier. V_T is the applied tunnel bias relative to the Fermi level ($E_{F'}$) of the substrate. In the case of a negative tip polarity shown here, electrons are injected from the Fermi level of the tip (E_F) into the empty level of the organic material.

in a highly localized fashion. The organic materials are self-assembled on the HOPG surface, which acts as the opposite electrode. The results of Sheats et al. indicated that the I−V characteristics of MEH−PPV obtained using Pt/Ir STM tips were in good agreement with those of the standard film devices.[24,25] In comparison to the photoemission spectroscopy techniques that have proved useful as probes of the occupied levels of organic materials,[26] the STS described herein has the unique capability that allows the direct measurement of molecular-level alignment of the filled and empty states of all the interfaces of a multilayer OLED. Scheme 3b shows the geometry and energy diagram for a typical STM configuration, in which charge injection into the organic material occurs via tunneling through a vacuum barrier.[27]

The strength of the electric field is much higher at the apex of a tip than at a planar electrode interface. To decrease this influence, the sharp tip was first deliberately pushed slightly into the substrate to form a relatively flat end. Spectroscopic data were acquired with the STM tip located over the self-assembled organic materials. Parallel experiments were also performed on the bare HOPG surface and on the alkane molecules to check the reliability of the spectra. The adsorption of the molecules on a weakly interacting substrate like HOPG ensures that the electronic structure of the molecules is only slightly distorted by the physisorption process as we observed in the STS spectra. To ensure reliability and high reproducibility, we collected a large number of curves to exclude artifacts, although acquisition of d*I*/d*V* spectra is a tedious task. Hundreds of curves were obtained for each system to exclude any possible artifacts. The presented d*I*/d*V* curves are the average of a selected number of curves to achieve the lowest signal-to-noise ratio. To further ensure the reliability of the experimental data, only those d*I*/d*V* curves for which clear STM images appeared again after the STS measurement were used for the analysis.

The averaged d*I*/d*V* curve obtained over the **BT** molecule in a large ordered **BT** domain on HOPG is plotted in Figure 7.

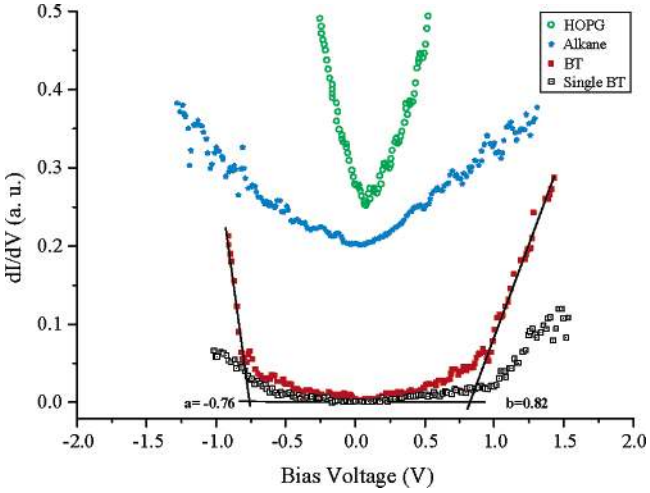

Figure 7. STS results of HOPG, alkane, BT, and single BT. For clarity, HOPG and alkane curves were vertically translated 0.2 a. u. toward positive direction. Tunneling conditions: $I = 336$ pA and $V = 1.09$ V.

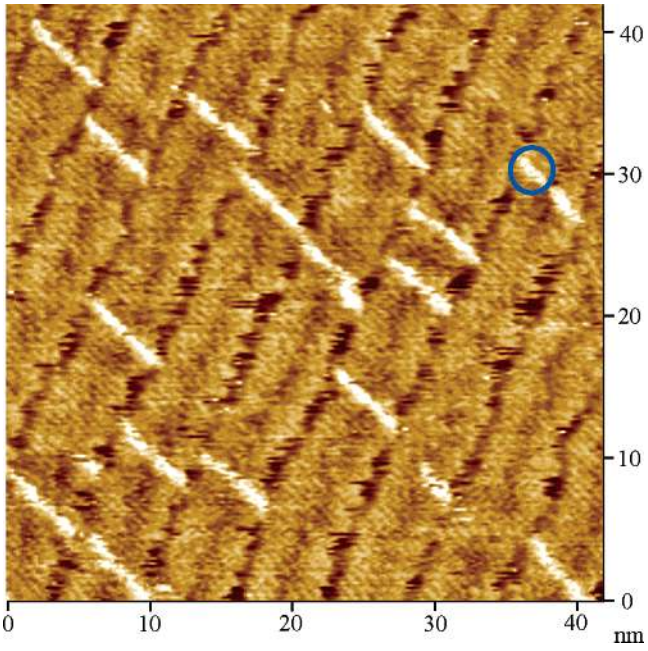

Figure 8. STM image of isolated BT molecules incorporated into the alkane matrix, recorded with $I = 336$ pA and $V = 1.09$ V. The circle incicates the single BT molecule.

The curve was made by acquiring consecutive spectra both over a **BT** molecule and over several molecules at different locations. The curve displays a discernible gap region around zero bias. The edges for the energy gap are determined by the position of an abrupt change in the slope of d*I*/d*V* versus *V* as indicated in Figure 7.[28] The d*I*/d*V* curve reveals that the measured gap ($\Delta = b-a$) between occupied states and unoccupied states is $\Delta_{BT} = 1.58 \pm 0.05$ eV. The offset of the Fermi level (the center position of the gap region) is calculated by the formula $\delta = (a + b)/2$, $\delta_{BT} = 0.06 \pm 0.02$ eV. On an alkane-modified HOPG surface as shown in Figure 8, a single isolated **BT** molecule can be seen as circled. Taking advantage of this phenomenon, the tunneling spectra were acquired over an individual **BT** molecule. The insertion method has been previously shown to be ideal for studying the electronic properties of isolated molecules.[29] The averaged d*I*/d*V* curve of an isolated individual **BT** in Figure 7 is similar to that of **BT** in a pure **BT** domain. This result can be explained by the molecular adsorption of **BT** to substrate. As the aromatic π system of **BT** is parallel to the underlying

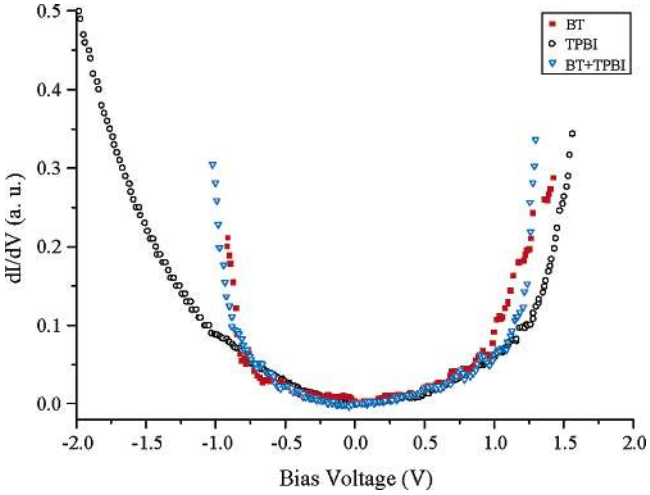

Figure 9. STS results of BT, TPBI, BT/TPBI mixed multilayer. Tunneling conditions: $I = 336$pA and $V = 1.09$ V.

surface, no face-to-face π stacking among **BT** molecules is formed. Therefore, the electronic property of isolated **BT** molecules on alkane-modified HOPG shows little change in comparison with those in the pure **BT** domain.

In contrast, the tunneling spectra acquired over the alkyl chains of the alkane adlayer and HOPG do not show a zero-conductance gap around the Fermi level. The curve over HOPG has a much sharper decrease in the slope (dI/dV) shown in Figure 7 (for clarity, these two curves were vertically translated 0.2 a. u. toward positive direction).[30] Note that the reproducibility of these spectra is good.

Figure 9 shows the average results of STS curves collected with the tip located over the self-assembled **TPBI** adlayer. Below E_F, the signal of the occupied states starts from ca. -1.28 eV, while above E_F the onset of the signal of the unoccupied states occurs at ca. 1.23 eV. Thus, the width of the measured gap is about 2.51 ± 0.05 eV, which is smaller than the bulk gap reported in the literature for **TPBI** (3.5 eV).[31] The difference in sample preparation, substrate, atmosphere under which the experiments are carried out, and dopant would greatly influence the gap value.[23] The measurement conditions for the value in the literature such as bulk TPBI (3.5 eV) produced by vacuum deposition and measure in a vacuum are different from the present conditions. In the present study, a self-assembling technique was employed in ambient atmosphere on the HOPG surface. The measurement was also carried out in ambient atmosphere. The difference of sample preparation, substrate, and the ambient atmosphere should be responsible for the value difference.

The averaged dI/dV curve obtained over the **BT/TPBI** mixed multilayer shows a band gap of 1.96 ± 0.05 eV in Figure 9, different from that of individual **BT** or **TPBI** layer. Some aspects of the doping effects have been simulated numerically.[32] When the doped layer is introduced, the trap charges are redistributed.

The same experiments were carried out over the **BT/TPBI** mixed multilayer heated to 80, 100, and 180 °C to study the annealing effect on the dI/dV curve. At 80 °C, phase separation already appeared in the mixed multilayer, so that the dI/dV could be recorded on either **BT** or **TPBI** adlayer. Comparing the curves with those obtained on the room-temperature sample, we observed no noticeable change in the dI/dV curves (not shown here), suggesting little change in the molecular electronic state. The results therefore suggest that the decay of OLED under heat treatment is caused by phase separation, which leads to the host−guest molecular distance beyond the available Förster's energy transfer distance R, rather than by the change of molecular electronic property.

Conclusion

We employed thermal treatment to simulate a Joule heating effect on the decay of OLED. The host molecule **TPBI** and guest molecule **BT** were prepared on an HOPG surface. The mixed **BT** and **TPBI** layer was considered to be a model of OLED luminescent layer. The structural changes, electronic spectroscopic properties, and PL of the assembled layers had been investigated by STM/STS and spectrofluorometry. It is found that **BT** and its derivative ***m*-BT** form an ordered pattern, and the methyl groups in ***m*-BT** result in a larger inter-row spacing than that of **BT**. Because of the steric configuration of **TPBI**, it is difficult for this host molecule to form two-dimensional ordered structures. **BT** and **TPBI** molecules mix homogeneously at room temperature, whereas at higher temperature, **BT** molecules migrate and agglomerate to form ordered domains. Aggregation of **BT** molecules in **TPBI** at higher temperatures might be one important cause of OLED decay, which is supported by the results of PL measurement. STS shows that the band gaps of **TPBI** and **BT** remain unchanged with annealing temperature. The result suggests that the decay of OLED under heat treatment is caused by an ineffective host−guest energy transfer. The direct microscopic observation afforded by STM measurements provided new insights into the degradation mechanism of OLED.

Acknowledgment. Financial support from the National Natural Science Foundation of China (No. 20025308 and 20103008), National Key Project on Basic Research (Grant G2000077501), and the Chinese Academy of Sciences is gratefully acknowledged. S.-T.L. acknowledges the financial support of Research Grants Council of Hong Kong SAR (Project No. CityU 2/02C). J.-R.G. is also in the Graduate School of CAS.

References and Notes

(1) Sheats, J. R.; Antoniadis, H.; Hueschen, M.; Leonard, W.; Miller, J.; Moon, R.; Roitman, D.; Stocking, A. *Science* **1996**, *273*, 884.
(2) Kraft, A.; Grimsdale, A. C.; Holmes, A. B. *Angew. Chem., Int. Ed.* **1998**, *37*, 402.
(3) Friend, R. H.; Gymer, R. W.; Holmes, A. B.; Burroughes, J. H.; Marks, R. N.; Taliani, C.; Bradley, D. D. C.; Dos Santos, D. A.; Brédas, J. L.; Lögdlund, M.; Salaneck, W. R. *Nature* **1999**, *397* (6715), 121.
(4) Baldo, M. A.; Thompson, M. E.; Forrest, S. R. *Nature* **2000**, *403*, 750.
(5) Ho, P. K. H.; Granström, M.; Friend, R. H.; Greenham, N. C. *Adv. Mater.* **1998**, *10*, 769.
(6) Sirringhaus, H.; Tessler, N.; Friend, R. H. *Science* **1998**, *280*, 1741.
(7) Cui, J.; Huang, Q.; Wang, Q.; Marks, T. J. *Langmuir* **2001**, *17*, 2051.
(8) Onitsuka, O.; Fou, A. C.; Ferreira, M.; Hsieh, B. R.; Rubner, M. F. *J. Appl. Phys.* **1996**, *80*, 4067.
(9) Goncalves-Conto, S.; Carrard, M.; Si-Ahmed, L. Zuppiroli, L. *Adv. Mater.* **1999**, *11* (2), 112.
(10) Brinkmann, M.; Gadret, G.; Muccini, M.; Taliani, C.; Masciocchi, N.; Sironi, A. *J. Am. Chem. Soc.* **2000**, *122*, 5147.
(11) Morita, T.; Kimura, S.; Kobayashi, S.; Imanishi, Y. *J. Am. Chem. Soc.* **2000**, *122*, 2850.
(12) Zheng, D.; Li, H.; Wang, Y.; Zhang, F. *Appl. Surf. Sci.* **2001**, *183*, 165.
(13) Yan, L.; Gao, Y. *Thin Solid Films* **2002**, *417*, 101.
(14) Liao, L. S.; He, J.; Zhou, X.; Lu, M.; Xiong, Z. H.; Deng, Z. B.; Hou, X. Y.; Lee, S. T. *J. Appl. Phys.* **2000**, *88* (5), 2386.
(15) Gong, J. R.; Lei, S. B.; Wan, L. J.; Deng, G. J.; Fan, Q. H.; Bai, C. L. *Chem. Mater.* **2003**, *15*, 3098.
(16) Alvarado, S. F.; Libioulle, L.; Seidler, P. F. *Synth. Met.* **1997**, *91*, 69.

(17) Zhang, X. H.; Wong, O. Y.; Gao, Z. Q.; Lee, C. S.; Kwong, H. L.; Lee, S. T.; Wu, S. K. *Mate. Sci. Eng. B* **2001**, *85*, 182.
(18) Chen, C. H.; Shi, J. *Coord. Chem. Rev.* **1998**, *171*, 161.
(19) Sato, Y.; Kanai, H. *Mol. Cryst. Liq. Cryst.* **1994**, *253*, 143.
(20) Shi, J. M.; Tang, C. W. *Appl. Phys. Lett.* **199**7, *70* (13), 1665.
(21) Ko, C.-W.; Tao, Y.-T.; Danel, A.; Krzeminska, L.; Tomasik, P. *Chem. Mater.* **2001**, *13*, 2441.
(22) Baldo, M. A.; O'Brien, D. F.; You, Y.; Shoustikov, A.; Sibley, S.; Thompson, M. E.; Forrest, S. R. *Nature* **1998**, *395*, 151.
(23) Ishii, H.; Sugayama, K.; Ito, E.; Seki, K. *Adv. Mater.* **1999**, *11* (8), 605.
(24) Sheats, J. R.; Chang, Y. L.; Roitman, D. B.; Stocking, A. *Acc. Chem. Res.* **1999**, *32*, 193.
(25) Parker, I. D. *J. Appl. Phys.* **1994**, *75*, 1656.
(26) Scudiero, L.; Barlow, D. E.; Mazur, U.; Hipps, K. W. *J. Am. Chem. Soc.* **2001**, *123*, 4073.
(27) Alvarado, S. F.; Rossi, L.; Müller, P.; Seidler, P. F.; Riess, W. *IBM J. Res. Dev.* **2001**, *45* (1), 89.
(28) Feenstra, R. M. *Phys. Rev. B* **1994**, *50*, 4561.
(29) Bumm, L. A.; Arnold, J. J.; Cygan, M. T.; Dunbar, T. D.; Burgin, T. P.; Jones, L., II; Allara, D. L.; Tour, J. M., Weiss, P. S. *Science* **1996**, *271*, 1705.
(30) Fan, X. L.; Wang, C.; Yang, D. L.; Wan, L. J.; Bai, C. L. *Chem. Phys. Lett.* **2002**, *361*, 465.
(31) Su, Y. Z.; Lin, J. T.; Tao, Y.-T.; Ko, C.-W.; Lin, S.-C.; Sun, S.-S. *Chem. Mater.* **2002**, *14*, 1884.
(32) Shen, J.; Yang, J. *SPIE* **1999**, *3621*, 86.